# Following Network Formation in an Epoxy/Amine System by Ultrasound, Dielectric, and Nuclear Magnetic Resonance Measurements: A Comparative Study

**R. E. Challis,[1] M. E. Unwin,[1] D. L. Chadwick,[2] R. J. Freemantle,[3] I. K. Partridge,[4] D. J. Dare,[2] P. I. Karkanas[4]**

[1]*School of Electrical and Electronic Engineering, University of Nottingham, NG7 2RD, United Kingdom*
[2]*Manchester Metropolitan University, M15 6BH, United Kingdom*
[3]*NDT Solutions, Limited, Dunston Innovation Centre, Chesterfield, S41 8NG, United Kingdom*
[4]*Department of Advanced Materials, Cranfield University, Bedford, MK43 0AL, United Kingdom*

Received 27 February 2002; accepted 12 June 2002

**ABSTRACT:** This article presents a comparison of data obtained from a low-temperature cure of an epoxy/amine system by three independent cure monitoring techniques: ultrasonic wave propagation, dielectric permittivity, and nuclear magnetic resonance. The sizes and thermal histories of the samples studied by the three techniques were controlled for comparability between the methods. The three techniques gave consistent information on the progress of cure and were complementary, in that each was particularly sensitive to different stages of the cure process. © 2003 Wiley Periodicals, Inc. J Appl Polym Sci 88: 1665–1675, 2003

**Key words:** thermosets; dielectric properties; NMR; ultrasound

## INTRODUCTION

The use of epoxy resins both as adhesives and as primary structural materials to form critical safety components and structures is now common in many industries, particularly in the aerospace and automotive sectors. In the interest of component quality and reliability and manufacturing process economy, there is a requirement for techniques to monitor the cure of the resins during the component forming process to provide essential quality assurance data[1,2] and eventually to provide the basis for real-time control of the process itself. Of particular interest is the identification of critical stages in the cure, such as gelation and vitrification.

Many physical methods have been applied to the monitoring of thermoset curing, principally in laboratory studies. Two prominent macroscopic methods are the measurement of dielectric permittivity[3–14] and the recording of ultrasonic wave propagation parameters, the most basic of which are the compression wave absorption coefficient and the phase velocity.[15–20] Another method that has frequently been applied is differential scanning calorimetry (DSC), either alone[21,22] or in combination with dynamic mechanical analysis (DMA),[23] dielectric measurements,[24] or ultrasonic studies.[25] Ultrasound has been combined with DMA and dielectric techniques by Matsukawa et al.[26] and with Brillouin scattering and photon correlation spectroscopy by Alig et al.[27] Low-resolution nuclear magnetic resonance (NMR) has been used alone[28] and in combination with ultrasound[29] to track the liquid–solid transition in a curing epoxy. Lovell and Windle[30] reported structural studies of epoxy cure with wide-angle X-ray scattering (WAXS), and we extended this work to compare observations of epoxy cure by WAXS, NMR, and ultrasound measurements.[31] Although all of these techniques could in principle be used to monitor a cure process, only the dielectric and ultrasonic methods have potential for applications in an industrial manufacturing setting because of cost, physical access, and safety. The purpose of this study was to investigate the similarity or complementarity of the dielectric and ultrasonic techniques when used to monitor the cure of an epoxy/amine resin system and to compare the results obtained from these two methods with a basic measure of the liquid–solid transition obtained from NMR data.

*Correspondence to:* R. E. Challis (richard.challis@nottingham.ac.uk).

Contract grant sponsors: UK Engineering and Physical Sciences Research Council; Leverhulme Trust.

Journal of Applied Polymer Science, Vol. 88, 1665–1675 (2003)


## EXPERIMENTAL

### Ultrasonic wave propagation

The phase velocity ($c$) and absorption coefficient ($\alpha$) for ultrasonic bulk wave propagation can be expressed

in terms of the real and imaginary parts of the elastic modulus governing propagation:[16,32]

$$c^2(\omega) = \frac{M_R(\omega)}{\rho} \tag{1}$$

$$\alpha(\omega) = \frac{\omega M_I(\omega)}{2\rho c^3(\omega)} \tag{2}$$

where $\omega$ is the angular frequency and $M_R(\omega)$ and $M_I(\omega)$ are the real and imaginary parts of the elastic modulus governing propagation, respectively. For shear waves, this is merely the shear modulus ($G$), whereas for compression waves, it takes a combined form ($K + 4G/3$, where $K$ is the bulk modulus). The mechanical loss tangent ($\tan \delta_M$) is given as follows:

$$\tan \delta_M = \frac{M_I}{M_R} = \frac{1}{\pi}\alpha(\omega)\lambda = \frac{2\alpha(\omega)c(\omega)}{\omega} \tag{3}$$

For a simple Debye process, $\tan \delta_M$ is a function of the unrelaxed and relaxed moduli ($M_\infty$ and $M_0$, respectively) and the mechanical time constant $\bar{\tau}_M$:[33]

$$\tan \delta_M = \frac{M_\infty - M_0}{(M_\infty M_0)^{1/2}} \frac{\omega\bar{\tau}_M}{1 + \omega^2\bar{\tau}_M^2} \tag{4}$$

Therefore, at a given time in the cure cycle, with locally stationary $\bar{\tau}_M$, we expect $\tan \delta_M$ as a function of frequency to peak at $\omega = 1/\bar{\tau}_M$. At a fixed frequency and with $\tan \delta_M$ a function of $\bar{\tau}_M$, a similar peak occurs, and so if $\bar{\tau}_M$ is expected to increase during the cure cycle, we would expect $\tan \delta_M$ to exhibit a peak as a function of time in the cure process. This can be interpreted as the passage of the center frequency of an $\alpha$-relaxation process through the measurement range. Therefore, at any time in the cure process, it is possible to estimate $\bar{\tau}_M$ from a knowledge of the frequency at which $\tan \delta_M$ reaches its peak value. The Debye model assumes a monodisperse molecular system in which a single time constant applies to deformations at all points in the material. Polydispersity in the molecular arrangement leads to a broadening of measured responses in frequency or time, frequently represented by, for example, a Cole–Cole[34] dependence on the frequency or cure time. Estimates of the developing relaxation time during a cure process made on the basis of the position of a peak in the measured data would still remain valid under the Cole–Cole model or related models.

### Ultrasonic measurements

The absorption coefficient and phase velocity of the ultrasonic waves in the curing samples were measured as functions of frequency with a novel goniometric system that has been described elsewhere[19] (Fig. 1). Both compression and shear wave data could be recorded quasisimultaneously during the cure of the resin samples at temperatures controlled in the range of 20–80°C (±0.5°C) and over frequency bandwidths within the range of 2–16 MHz. The instrument used conventional ultrasonic compression wave transducers (tmp3, Sonatest, Plc., Milton Keynes, United Kingdom) connected to a commercial pulse receiver (UPR-1, NDT Solutions, Ltd., Chesterfield, United Kingdom). Raw signals were digitized at 400 MHz with a digital storage oscilloscope (S9410, LeCroy Corp., Chestnut Ridge, NY) connected via a standard interface (GPIB, IEEE 488, NT-488.2, National Instruments Corp., Austin, TX) to a Pentium personal computer for instrument control and signal processing. Ultrasonic wave attenuation and phase velocity as functions of frequency were calculated with conventional Fourier techniques. The time required for a combined compression and shear wave measurement over the full frequency bandwidth was 50 s, which allowed for the required mechanical resetting of the goniometer angle. The material was cured at 25°C, and recordings were made at intervals of 2 min over a cure time of 150 min.

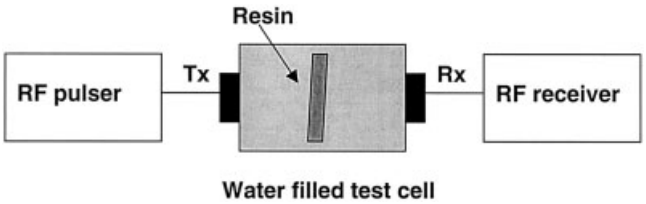


**Figure 1** Schematic of the ultrasound test cell with a sample in place.

### Dielectric phenomena

The relative permittivity ($\epsilon^*$) of a curing resin can be expressed as the following complex quantity:

$$\varepsilon^* = \varepsilon' - i\varepsilon'' \tag{5}$$

where $\varepsilon'$ and $\varepsilon''$ are, respectively, the real and imaginary parts, and $i$ is $(-1)^{1/2}$. It derives from the sum of responses due to electronic and atomic effects, ionic conduction, and induced and static dipoles (for an example, see ref. 35). Although not active in the bulk resin material, electrode polarization also contributes to measured responses. In phase-separated mixtures, there is an additional component due to interfacial polarization. The contribution of the electronic effects is approximately three units. The effects of ionic conduction show as a loss component in the dielectric response with a reciprocal dependence on frequency:

$$\varepsilon''_c = \frac{\sigma}{\omega \varepsilon_{fs}} \tag{6}$$

where $\varepsilon''_c$ is the loss component, $\sigma$ is the conductivity and $\epsilon_{fs}$ is the permittivity of free space. The ionic conductivity is proportional to the ion mobility and concentration and varies approximately inversely with the viscosity of the resin. The dipolar contribution results from rotational diffusion of the molecular dipole moments. It is associated with relaxation processes in the resin material in a manner that is analogous to the mechanical case outlined previously. It is convenient to quantify the dielectric loss in terms of the dielectric loss tangent (tan $\delta_E$), which can be expressed in a form similar to the mechanical case given in eqs. (3) and (4):

$$\tan \delta_E = \frac{\varepsilon''}{\varepsilon'} \tag{7}$$

The loss tangent can be expressed as a function of frequency, which for a simple Debye process gives[33]

$$\tan \delta_E = \frac{\varepsilon_0 - \varepsilon_\infty}{(\varepsilon_0 \varepsilon_\infty)^{1/2}} \frac{\omega \bar{\tau}_E}{1 + \omega^2 \bar{\tau}_E^2} \tag{8}$$

where $\bar{\tau}_E$ is the electrical time constant[33] and $\epsilon_\infty$ and $\epsilon_0$ are the unrelaxed and relaxed permittivities, respectively. Therefore, tan $\delta_E$ expressed as a function of frequency at a point in the cure or as a function of time at a given frequency would be expected to exhibit a peak at $\omega \bar{\tau}_E = 1$ analogously to the mechanical case given earlier. Again, the molecular polydispersity can be handled by extensions to the Debye formulation such as the Cole–Cole model.[34]

The outlined relationships provide an important basis for monitoring the cure of a resin system. At the beginning of the cure, when the viscosity is relatively low, the imaginary part of the dielectric permittivity is high because of ionic conductivity in the liquid resin. As the cure proceeds and the viscosity increases, the conductivity decreases sharply but does not reach zero even after gelation. The contribution to the dielectric loss due to dipolar relaxation appears as an imaginary part to $\epsilon^*$ and a developing loss tangent that reaches a maximum at $\omega \bar{\tau}_E = 1$; $\bar{\tau}_E$ increases as the molecular size increases, and so the maximum in tan $\delta_E$ occurs at successively lower frequencies as the cure proceeds. As with the mechanical case, these changes in $\bar{\tau}_E$ represent an $\alpha$ relaxation and are related to changes in the glass-transition temperature ($T_g$) of the resin; it has been shown that log $\bar{\tau}_E$ is proportional to $T_g^2$, and for a constant cure temperature, the log increases approximately linearly with the cure time.[7] A logarithmic plot of the relaxation frequency ($1/\bar{\tau}_E$) versus the cure time, extrapolated to 1 Hz, gives a useful estimate of the cure time for vitrification of the resin.[9] In relation to the real part of the dipolar contribution to permittivity, it has been found that the low frequency value $\epsilon_0$ decreases during the cure and decreases with temperature; the high frequency value $\epsilon_\infty$ is independent of the cure time and temperature and typically falls between values of two and four units.

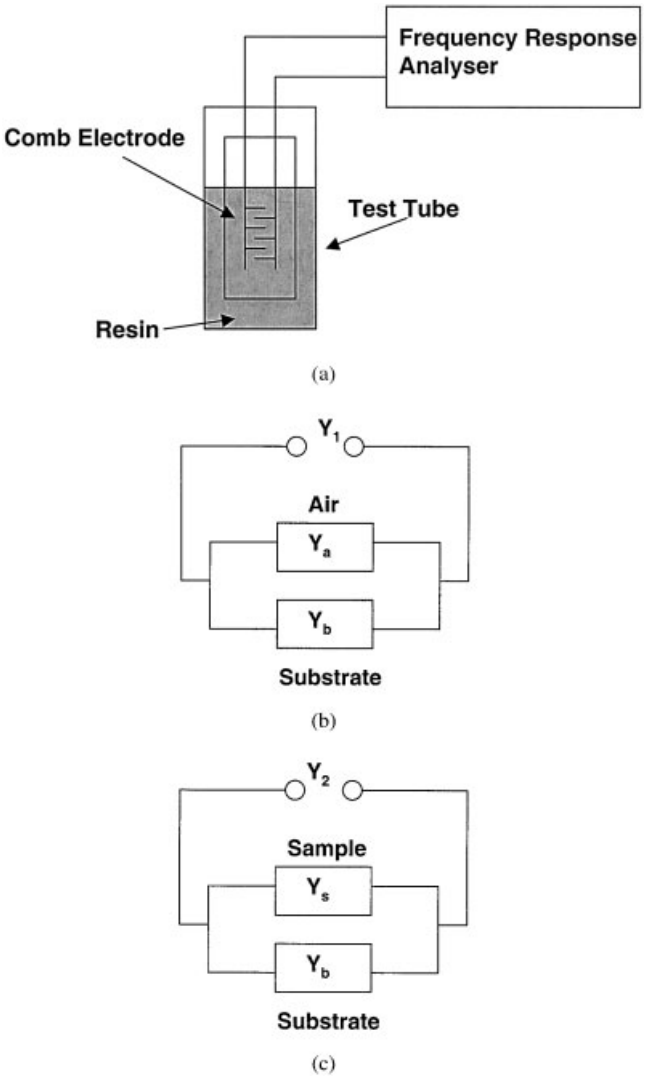


**Figure 2** Schematic of (a) the dielectric test cell with a sample in place, (b) the circuit with the electrode assembly in air, and (c) the circuit when inserted into the sample.

## Dielectric measurements

Measurements of the dielectric permittivity *in situ* in a curing resin typically involve an interdigitating comb electrode laid down on a polymer substrate that is first characterized in air and then inserted into the sample precure[9] [Fig. 2(a)]. The complex admittance of the electrode system is characterized over the frequency range of interest in air, at the temperature at which the

cure will take place. With reference to Figure 2(b), this gives

$$Y_1 = Y_a + Y_b = Y_1' + iY_1'' \tag{9}$$

where $Y_a$ is the component due to the electric field in air and $Y_b$ is due to the field in the polymer substrate. It is assumed that the electrode fingers are on the boundaries of the two half-spaces (air/substrate):

$$Y_b = \varepsilon_b^* Y_a \tag{10}$$

where $\epsilon_b^*$ is the complex permittivity of the substrate. It follows that

$$Y_1 = (1 + \varepsilon_b^*) Y_a \tag{11}$$

When the electrode is placed in the sample [Fig. 2(c)], the terminal admittance is

$$Y_2 = (\varepsilon_s^* + \varepsilon_b^*) Y_a = Y_2' + iY_2'' \tag{12}$$

where $\epsilon_s^*$ is the complex permittivity of the sample.

The substrate materials are chosen to have low loss so we can assume $Y1'' \gg Y1'$ and $\epsilon_b'' \ll \epsilon_b'$. The manipulation of eqs. (9)–(12) then yields the real and imaginary parts of the sample permittivity:

$$\varepsilon_s' = \frac{Y_2''}{Y_1''}(1 + \varepsilon_b') - \varepsilon_b' \tag{13}$$

$$\varepsilon_s'' = \frac{Y_2'}{Y_1''}(1 + \varepsilon_b') \tag{14}$$

In the experiments described later, $\epsilon_s''$ was used to track the ionic conductivity component and the dipolar components of dielectric loss in the curing material. The dielectric sensors had interdigitating electrodes with an element spacing of 300 $\mu$m on a substrate 70 $\mu$m thick (DekDyne Inc., Williamsburg, VA). The sensors were connected to a frequency response analyzer (SI 1260, Solartron) described in an earlier work[7,9] and augmented by a dielectric interface (SI 1296, Solartron Analytical, Farnborough, UK) to enable measurements of currents of the order nanoampères as the conductivity of the curing resin was reduced to very low values toward the end of the cure. The output of the system was the complex admittance of the test piece as a function of frequency. The measurement frequency range was between 0.3 Hz and 1 MHz. At the start of each experiment, measurements were made of the admittance of the circuit between the instrument and the sensor and then of the admittance with the sensor connected but held in air so that the permittivity of the sensor substrate could be obtained. The sensor was then inserted into a thick (2-mm) layer of the uncured resin–hardener mixture set in an oven held at 25°C, and wide bandwidth admittance recordings were made at intervals of 2 min over a cure time of 150 min.

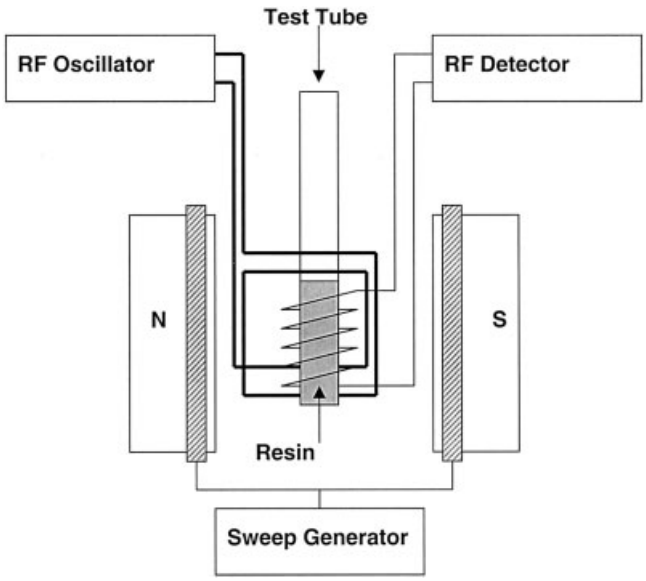


**Figure 3** Schematic of the NMR test cell with a sample in place.

### NMR measurement technique

The apparatus and rationale for NMR measurements on curing resins have been the subject of earlier publications,[28,29,31] and the same techniques were applied in this work. The apparatus is sketched in Figure 3. The instrument used (P120 Minispec, Brucker, Biospin Corp., Billerica, MA) was tuned to 20 MHz and had a permanent magnet of 4.7 kG ± 10 G. It was sensitive to spin relaxations of hydrogen nuclei bound at specific sites in the resin, hardener, and resin–hardener molecules. Short-pulse radiation applied to the sample resulted in decaying radio frequency signals after the relaxation of excited nuclei. These were processed to extract the amplitude–time signal, that is, the free induction decay (FID), which was analyzed into two exponential basis functions, each characterized by a decay time constant and an initial amplitude. For protons bound in molecules forming a liquid phase, such as the uncured resin and hardener, the decay time constant $T_{2l}^*$ is generally of the order of milliseconds. For protons bound in the solid phase of the curing resin, the time constant $T_{2S}^*$ is much shorter, typically of the order of 10 $\mu$s. FID signals from a curing resin system contain components with time constants in the liquid range and with others in the solid range corresponding to the cured material. The composite signal [$y(t)$] can be described as follows:

$$y(t) = A_l(e^{-t/T_{2l}^*})^2 + A_s(e^{-t/T_{2s}^*})^2 \tag{15}$$

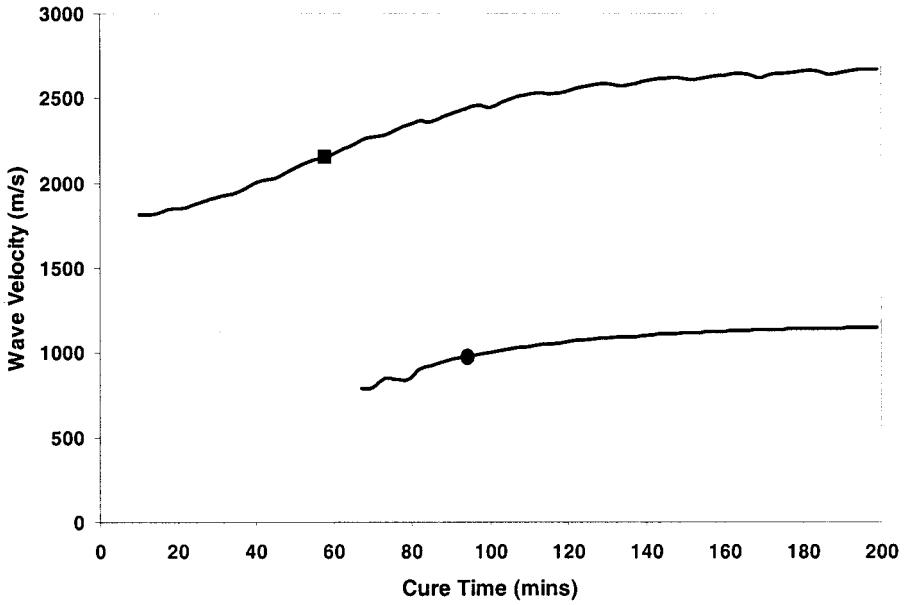


**Figure 4** Measured (■) ultrasonic compression and (●) shear wave velocities at 10 MHz as functions of the cure time.

where $A_l$ and $A_s$ are the partial signal amplitudes that correspond, respectively, to the liquid and solid material contributions to the FID. $T_{2l}^*$ and $T_{2s}^*$ are the corresponding time constants that characterize the two components of the decay. The FID is processed by means of a least mean square (LMS) fitting algorithm that extracts $A_l$, $T_{2l}^*$, $A_s$, and $T_{2S}^*$ from the composite signal. The magnitude of $A_l$ gives a measure of the fraction of uncured molecules in the liquid state, whereas $A_s$ gives the measure of the fraction of large macromolecules forming the solid components in the mixture. The changing magnitudes of $A_l$ and $A_s$ during the cure reaction enables the transition from liquid to solid in the curing material to be observed as a function of time. In this work, this analysis was performed at intervals of 3 min from the time at which the uncured resin mixture was transferred to the NMR instrument for a duration of 150 min.

### Resin material and experimental protocol

The resin used was an unmodified bisphenol A (AY105, Ciba Polymers, Duxford, United Kingdom), and the hardener was an accelerated aliphatic polyamine containing 50–62% diethylenetriamine (HY2958, Ciba Polymers). This resin–hardener system was chosen because preliminary studies had indicated that it was not prone to bubble formation, which would compromise the ultrasonic study, and that the cure could be successfully monitored by all three of our techniques. The sample preparation was synchronized to establish a common starting time and conditions for all three techniques. The resin and hardener samples were warmed in an oven to the curing temperature of 25°C for 30 min before being mixed so that they matched the operating temperature of the instruments. The material was mixed into 20-g batches, the time at which mixing began being taken as time zero in the cure process. Samples of 1–2 g were then placed in the measurement cells of the three different apparatus sets, and the cure was monitored for 150 min. Samples of such volumes exhibited minimal exotherms during cure.

## RESULTS

Figure 4 shows the development of the compression and shear wave velocities, calculated at 10 MHz, plotted against the cure time. The compression wave velocity follows a sigmoidal curve and indicates the development of $M_R(\omega)$ , reaching a stable value at the end of the cure. Such development of the elastic modulus in a curing material is typical of autocatalytic cure mechanisms. It was not possible to observe shear waves early in the cure because such waves remain evanescent in liquid materials. However, around 70 min into the cure, shear waves were just observable as solid material began to form; the subsequent increase in the shear wave velocity followed the development of $G$ as solidification progressed. Figure 5 shows the absorption coefficients calculated for both wave types at 10 MHz as functions of the cure time. When shear waves are first observed, the absorption is high; this indicates that the imaginary part of $G$ is high because of the strongly viscoelastic nature of the partly cured material. Toward the end of the cure, the shear wave absorption falls rapidly as vitrification takes place, and the imaginary part of $G$ decreases as its real part increases. The compression wave absorption rises to a peak around 30 min corresponding to the condition

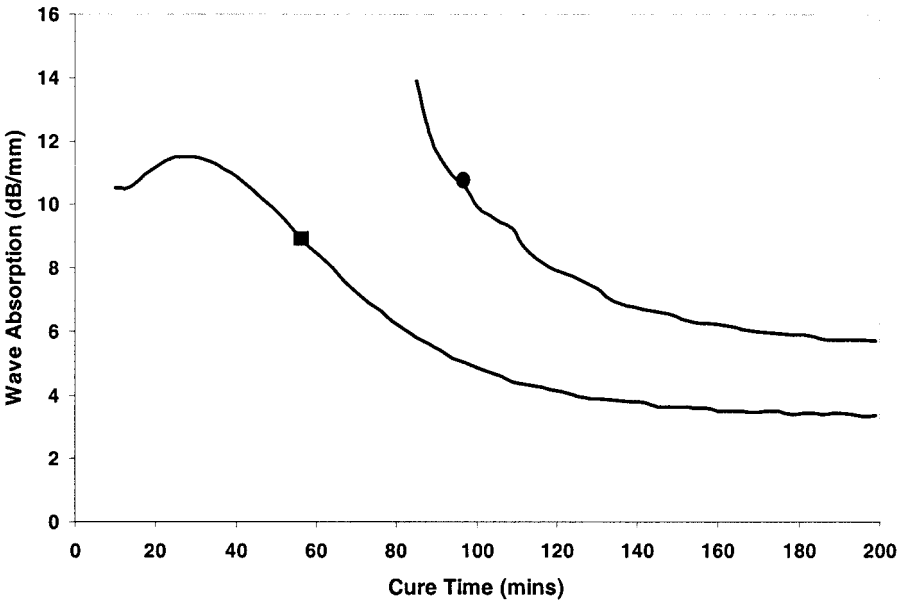


**Figure 5** Measured (■) ultrasonic compression and (●) shear wave absorption at 10 MHz as functions of the cure time.

$\omega\bar{\tau}_M = 1$ at 10 MHz for a relaxation process. The residual absorption in the cured material is thought to result from $\beta$-relaxation processes associated with the motions of short molecular segments.

Figure 6 shows the compression wave loss tangent as a function of the cure time plotted for three frequencies in the measurement range. The maximum time on the horizontal axis of this graph has been limited to 120 min so that the small shift of the peak value to the left as the frequency increases can be observed. The relaxation times corresponding to $1/2\pi f$, where $f$ is the frequency of the curves in Figure 6, are compared later to the dielectric relaxation times shown in Figure 10. The real and imaginary parts of the dielectric permittivity as a function of the cure time for three frequencies are shown in Figure 7. The very high values of the imaginary part at the initiation of the cure and the sharp fall in the early stages of the cure are due to the effects of ionic conduction in the still liquid material and indicate a rapid increase in its viscosity during the first 10 min of the cure cycle. The peak values occurring around 53 min at 10 kHz and around 40 min at 56 kHz correspond to the $\alpha$ relaxation associated with dipolar motion. Tan $\delta_E$ [eqs. (7)

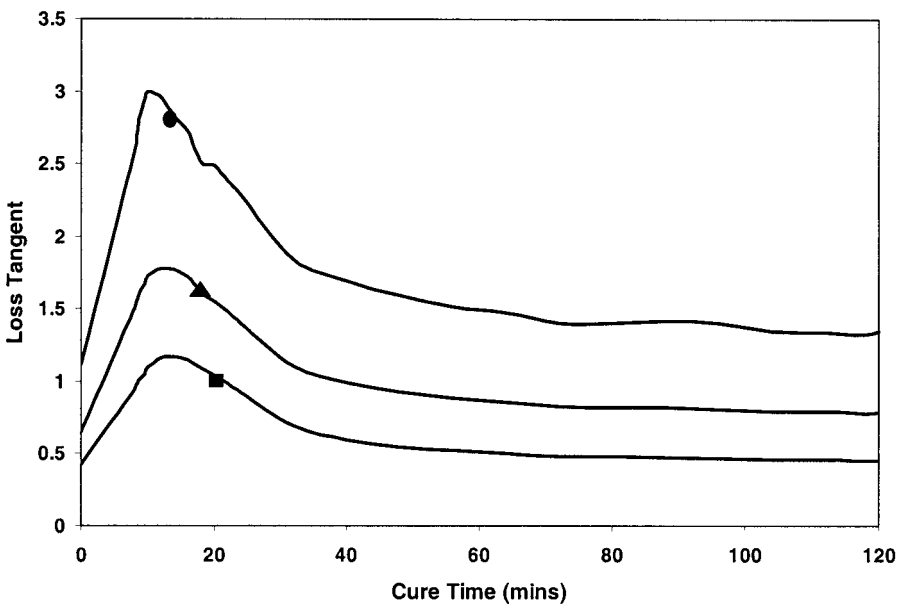


**Figure 6** Ultrasonic compression wave loss tangent at (■) 5, (▲) 8, and (●) 13 MHz as a function of the cure time.

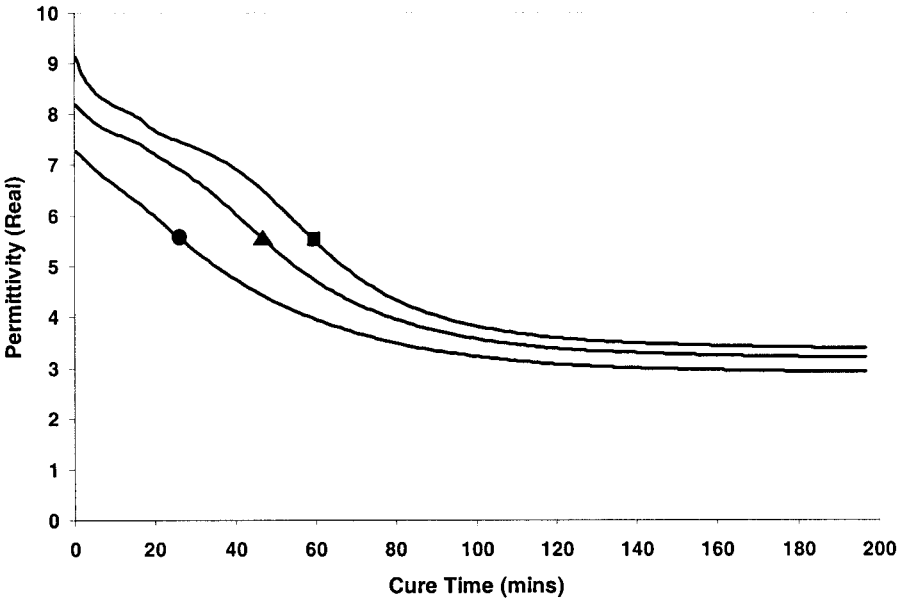


(a)

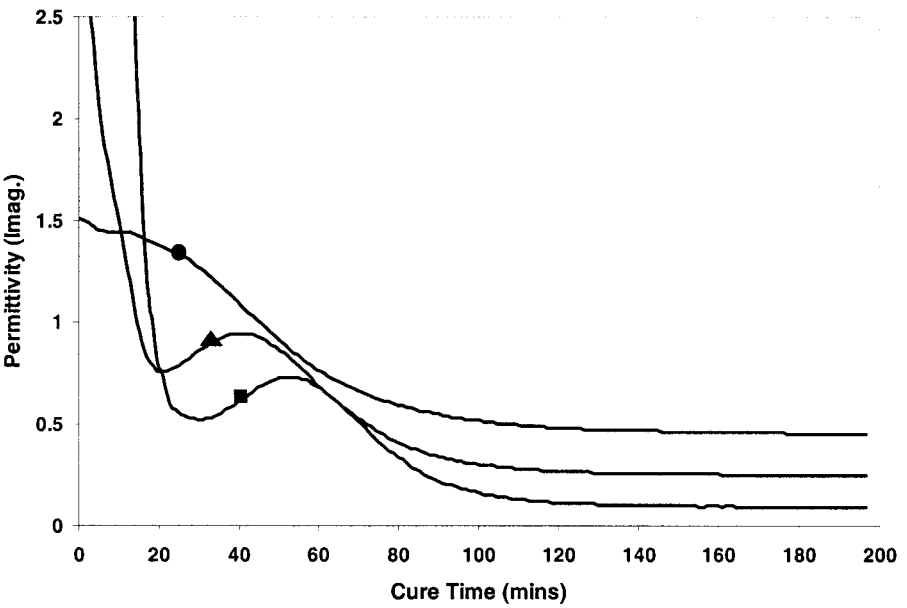


(b)

**Figure 7** (a) Real and (b) imaginary parts of the dielectric permittivity at (■) 10, (▲) 56, and (●) 560 kHz as functions of the cure time.

and (8)] is plotted in Figure 8 versus the cure time for the same three frequencies. As with the ultrasonic compression wave data (Fig. 6), we note a peak in the tangent that occurs earlier in the cure as the frequency increases and that is, again, typical of the passage of the $\alpha$ relaxation through the measurement frequency–time interval as the cure proceeds. The value of the conductivity calculated from eq. (6) and corresponding to the loss peaks in Figure 6 is plotted versus the cure time in Figure 9, in which it is seen to decrease as the cure proceeds. There is an inflection in the curve around 57 min into the cure, which is consistent with earlier results[7,9] and is close to the expected gelation time of the resin–hardener mixture used. The further inflection around 100 min corresponds to the completion of the solidification process as observed by NMR (discussed later). The relaxation times corresponding to the peaks in tan $\delta_E$ for a range of frequencies (Fig. 6) are plotted versus the cure time in Figure 10 with the ultrasonically determined relaxation times superimposed. Although the ultrasonic measurements were restricted to a relatively small range of frequencies

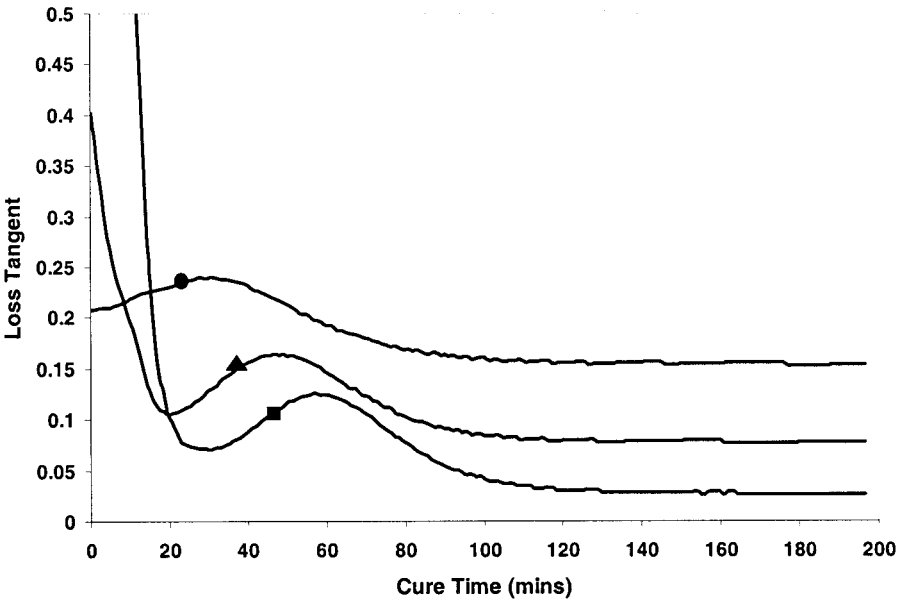


**Figure 8** Tan $\delta E$ at (■) 10, (▲) 56, and (●) 560 kHz as a function of the cure time.

and, therefore, relaxation times, Figure 10 gives some evidence that the ultrasonic and dielectric relaxation times follow the same trajectory, although the rate of change of the ultrasonic data appears to be higher than that of the dielectric data.

The NMR–FID exponential amplitudes are plotted against the cure time in Figure 11, one representing the liquid fraction of the curing mixture and the other the solid fraction. During the first 20 min of the cure, the curves are relatively flat, indicating little change in proton mobility. This is consistent with an initial reaction in a liquid phase during which epoxy groups and amine groups react to produce an alcoholic hydroxyl and a secondary amine. After 20 min, the transition to the solid accelerates, with a consequent reduction in proton mobility. This is consistent with reactions between alcoholic hydroxyls and secondary amines and the initiation of network formation. The crossover point for the liquid and solid amplitude signals occurs at 55 min, which is close to the occurrence of the inflection observed in the conductivity data at 57 min. The short transient in the NMR data around 65 min we attribute to a hydrogen-exchange reaction between a partially reacted secondary amine from the hardener and an alcoholic hydroxy

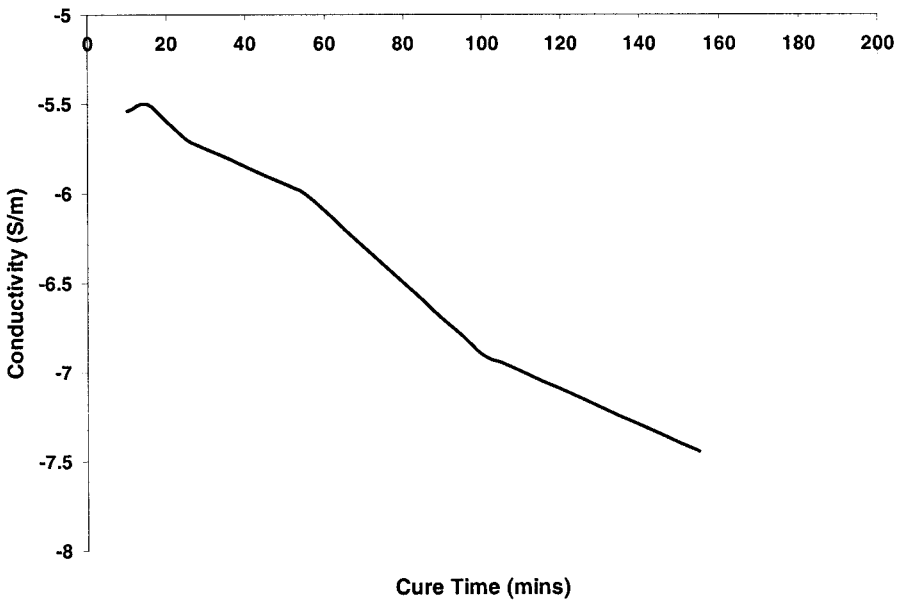


**Figure 9** Conductivity as a function of the cure time.

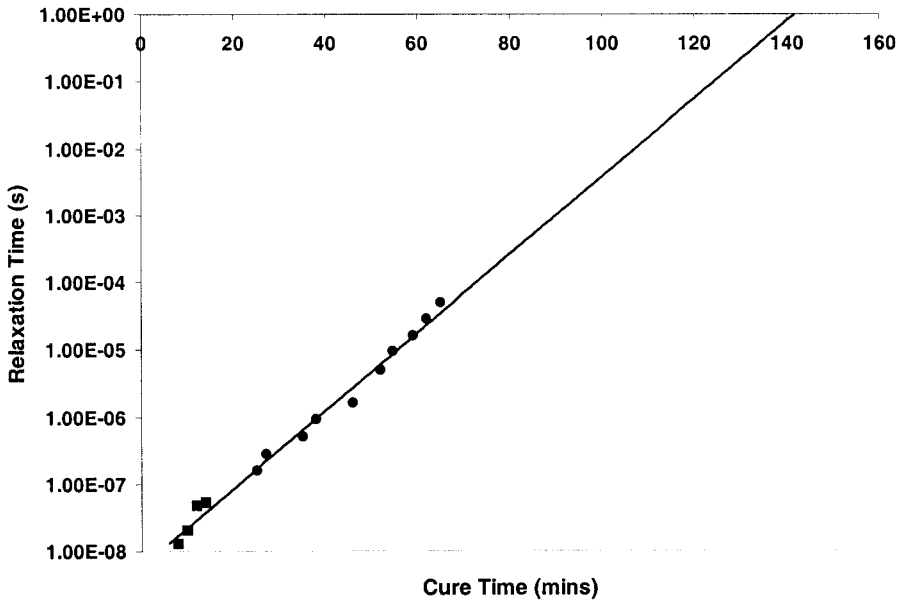


**Figure 10** Dielectric (●) and ultrasonic (■) relaxation times as functions of the cure time. A straight line has been fit to all the data, and extrapolation to a relaxation time of 0.1595 min, equivalent to a relaxation frequency of 1 Hz, gives an estimate of the vitrification time of 127 min.

group from a reacted epoxide ring from the resin. After 70 min or so of reaction, the rate of conversion from liquid to solid slows down. This is consistent with a reduction in the concentration of secondary amines and alcoholic hydroxyls as network formation continues. The conversion from liquid to solid appears to be complete around 100 min, when the liquid signal falls close to zero.

## DISCUSSION

Earlier work of ours has described the monitoring of resin cure by dielectric,[8,9] ultrasound,[16,19,31] and NMR techniques.[28,29] The aim of this article is to demonstrate the complementary nature of these three techniques when they are applied to the same resin–hardener system. The previously described results for the three techniques demonstrate definable stages of cure that are characterized by features in the measured data. We consider these features in the context of three stages of cure.

### Stage 1: liquid phase (0–20 min)

During the early stage of cure, there was very little change in the NMR data (Fig. 11), and this indicated a

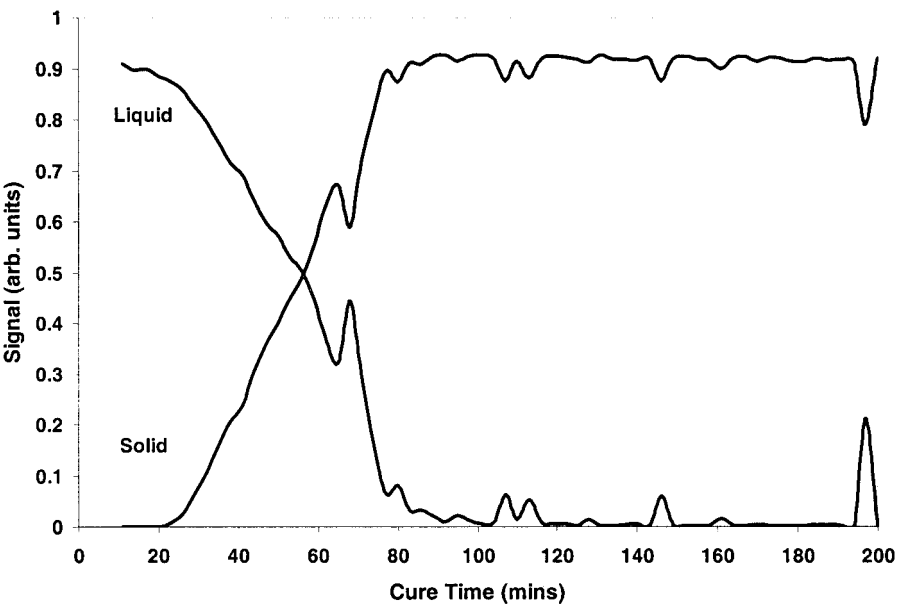


**Figure 11** Measured NMR solid and liquid signal amplitudes as functions of the cure time.

continuing liquid state with no change in proton mobility observable. However, the conductivity data (Fig. 9) showed a consistent fall, and tan $\delta_E$ (Fig. 8) also fell rapidly; this indicated increasing viscosity and decreased ionic mobility in general. The dielectric $\alpha$-relaxation peak could not be assessed during this interval, it being masked by high values of conductivity. Ultrasonic shear waves were not observed, and this again confirmed the liquid state (Fig. 4). The ultrasonic compression wave velocity (Fig. 4) began to increase slowly in the interval, indicating an initial slow increase in the bulk modulus in the material as the cure reaction got under way. The peaks in the ultrasonic compression wave loss tangent (Fig. 6) attributable to the relaxation were observable from about 10 min into the cure, and it can be seen from Figure 10 that the corresponding relaxation times increased relatively rapidly in the interval from 8 to 20 min. This would imply a high rate of molecular growth despite the continuing liquid state and only slow changes in the bulk modulus. The ultrasonic relaxation times were not measurable earlier than about 10 min because the corresponding frequencies were above the 16-MHz upper limit available with this test cell. However, extrapolation by the naked eye back to the zero time on the curve shown in Figure 10 suggests that the initial acoustic relaxation time in the liquid material was in the range of 1–3 ns. This stage in the cure can be summarized as a liquid one in which there is rapid molecular growth, rapidly diminishing conductivity, and relatively slow development of bulk mechanical properties.

### Stage 2: gelation (20–70 min)

The NMR data in Figure 11 show a rapid reduction in the liquid curve and a rapid rise in the solid curve, indicating that the environment for excitable hydrogen nuclei was changing rapidly from being liquidlike to solidlike. The intersection of the two curves at 55 min can be taken to indicate gelation. The rapid fall in conductivity (Fig. 9) gives further evidence of solidification, and the inflection in the curve around 57 min provides evidence for gelation at that time,[7,9] corroborating the NMR results. Ultrasonic shear waves became observable around the same time (Fig. 4); this indicated the establishment of $G$, initially with a high imaginary part leading to high absorption (Fig. 5). The compression wave velocity increased gradually through the period with no significant inflections, indicating a steady growth of the real part of the compression modulus. The maximum rate of change in this curve occurred around 57 min, which corresponded to the expected gelation time. The peaks in the ultrasonic loss tangent were not observable during this interval because the relaxation frequencies were below 2 MHz, which was the minimum measurable with the test cell used for our experiments. However, the ultrasonic loss tangent curves (Fig. 6) were seen to fall and approach nearly stationary values during this interval, as did the tan $\delta_E$ curves, only at longer times because of the lower measurement frequencies. The rapid growth in the relaxation times (Fig. 10) slowed in the first part of this interval but increased slightly around 50 min, which was close to the gelation time observed from the conductivity and other ultrasonic data. In summary, this stage of cure is dominated by gelation, a reduction in conductivity, the initial ability to support shear, and the gradual development of elastic moduli with diminishing imaginary parts.

### Stage 3: postgelation and vitrification (70 min onward)

The NMR curves (Fig. 11) reached saturation values, which indicated that all of the material was solid in the context of the mobility of bound hydrogen nuclei. The dielectric permittivity and loss tangents rapidly approached their end-of-cure values, indicating a significant reduction in the rate of reaction. The ultrasonic data shown in Figures 4–6 reflect the same phenomena with a slowing of the rate of change of all measured variables. However, significant development of elastic moduli was still observed for both compression and shear waves, and the measurable changes in absorption for both wave modes indicated a continuing development in the mechanical properties at times when the raw dielectric data were relatively featureless. We attribute these changes in elasticity to the growth of molecular crosslinking and observe that ultrasonic data appear to be more sensitive to changes during this stage of cure than data from either dielectric or NMR recordings. We infer from these results that at this stage in the cure, relatively small chemical changes (the number and type of bonds) had a disproportionately large influence on the development of the mechanical properties of the material. Beyond 150 min, we observed that the mechanical properties continued to change slightly for periods of up to 24 h, and this indicated some chemical changes in the material over this period. Previous work has shown[8] that the extrapolation of the dielectric relaxation frequency to 1 Hz on a frequency/cure-time plot gives an indication of the time to vitrification of the material. This is based on the assumption that the logarithm of the relaxation frequency follows the time into cure in a linear fashion. A reference to Figure 10 shows that the ultrasonic relaxation times appeared to change more rapidly very early in the cure and that the observed dielectric relaxation times followed a linear curve except for a small inflection around the gel time, between 40 and 60 min. However, notwithstanding these observations, we have fitted a straight line to all of the relaxation time data in Figure 10. This intersected the re-

laxation time value of $1/2\pi = 0.159$ s at a cure time of 127 min that we, therefore, take as the time to vitrification for the material at the cure temperature used. We note that after this time, the compression wave velocity was yet to increase by a further 4% and the shear velocity was yet to increase by a further 7%. This indicated further increases in the compression and shear moduli of around 8% and 14%, respectively.

## CONCLUSIONS

The cure of a bisphenol A resin system has been characterized with three complementary techniques: ultrasound, dielectric, and NMR. Diagnostic features in the data from each of the methods have been related to three principal stages in the cure process. The bandwidth of the apparatus available for the dielectric measurements was limited to an upper frequency limit of 1 MHz, whereas the bandwidth of the ultrasound system was restricted to the 2–16-MHz range by the responses of the transducers used. With this apparatus, it was not possible to use different sets of transducers to extend the bandwidth either downward because of errors associated with transducer aperture diffraction or upward because of a diminishing signal-to-noise ratio that resulted from higher absorption in the adhesive at higher frequencies. Although the two techniques could be said to be truly complementary in the context of these experiments, we note that the slope of the ultrasound relaxation time data was different from that of the dielectric data, although the two functions appeared to lie on a continuous curve. For the future, there will, therefore, be value in repeating part of this work for both dielectric and ultrasonic measurements up to 20 MHz or so to investigate whether the two techniques are sensitive to the same or different relaxation processes early in the cure. It will also be instructive to complement the existing study with a time plot of measures of conversion, such as DSC or Fourier transform infrared, neither technique being available at the time at which the experiments described here were performed. An ultrasonic system operating well below 1 MHz would, in principle, provide useful data on the later stages of cure in processes for which DMA could not be applied, although low-frequency ultrasound techniques applied to small samples are fraught with problems due to the effects of diffraction, vibration mode conversion, and standing waves. However, overall it has been shown that key diagnostic features in the data from each method are corroborated by equivalent features in the other two methods, although ultrasound seems to be the most sensitive to changes around and after vitrification. This study demonstrates that in cases for which one technique may be most suitable for an engineering application, comparative results obtained on a laboratory scale from the other techniques can aid in the interpretation of subsequent data obtained in the process.

The authors acknowledge with thanks G. M. Maistros for discussions concerning the interpretation of the dielectric data.

## References

1. Kent, R. N. In Comprehensive Composite Materials; Kelly, A.; Zweben, C., Eds.; Elsevier: New York, 2000; Chapter 5.18.
2. Griffith, J. M.; Hackett, T. Proceedings of the 45th International SAMPE Symposium, Covina, CA, May 21–25, 2000; SAMPE.
3. Williams, G.; Watts, D. C. Trans Faraday Soc 1970, 66, 80.
4. Senturia, S. D.; Sheppard, N. F., Jr. Adv Polym Sci 1986, 180, 1.
5. Mangion, M. B. M.; Johari, G. P. Macromolecules 1990, 23, 3687.
6. Lairez, D.; Emery, J. R.; Durrand, D.; Hayward, D.; Pethrick, R. A. Plast Rubber Compos Process Appl 1991, 16, 231.
7. Mangion, M. B. M.; Johari, G. P. J Polym Sci Part B: Polym Phys 1991, 29, 1127.
8. Maistros, G. M.; Block, H.; Bucknall, C. B.; Partridge, I. K. Polymer 1992, 33, 4470.
9. Maistros, G. M.; Partridge, I. K. Compos Sci Technol 1995, 53, 355.
10. Butta, E.; Livi, A.; Levita, G.; Rolla, P. A. J Polym Sci Part B: Polym Phys 1995, 33, 2253.
11. Fournier, I.; Williams, G.; Dutch, C.; Aldridge, G. A. Macromolecules 1996, 29, 7097.
12. Williams, G.; Smith, I. K.; Holmes, P. A.; Varma, S. J Phys: Condens Matter A 1999, 11, 57.
13. Karkanas, P. I.; Partridge, I. K. J Appl Polym Sci 2000, 77, 1419.
14. Karkanas, P. I.; Partridge, I. K. J Appl Polym Sci 2000, 77, 2178.
15. Lindrose, A. M. Exp Mech 1978, 18, 227.
16. Challis, R. E.; Alper, T.; Holmes, A. K.; Cocker, R. P. Meas Sci Technol 1991, 2, 59.
17. Alig, I.; Lellinger, D.; Johari, G. P. J Polym Sci Part B: Polym Phys 1992, 30, 791.
18. Matsukawa, M.; Nagai, I. J Acoust Soc Am 1996, 99, 2110.
19. Freemantle, R. J.; Challis, R. E. Meas Sci Technol 1998, 9, 1291.
20. Maffezoli, A.; Quarta, E.; Luprano, V. A. M.; Montagna, G.; Nicolais, L. J Appl Polym Sci 1999, 73, 1969.
21. Jenninger, W.; Shawe, J. E. K.; Alig, I. Polymer 2000, 41, 1577.
22. Alig, I.; Jenninger, W.; Shawe, J. E. K. J Non-Cryst Solids 1998, 235, 504.
23. Nguyen, N. T.; Lethiecq, M.; Gerard, J. G. Ultrasonics 1995, 33, 323.
24. Alig, I.; Jenninger, W.; Shawe, J. E. K. Thermochim Acta 1999, 330, 167.
25. Alig, I. Thermochim Acta 1997, 304, 35.
26. Matsukawa, M.; Okabe, H.; Matsushige, K. J Appl Polym Sci 1993, 50, 67.
27. Alig, I.; Lellinger, D.; Nancke, K.; Rizos, A.; Fytas, G. J Appl Polym Sci 1992, 44, 829.
28. Dare, D. J.; Chadwick, D. L. Int J Adhes Adhes 1996, 16, 155.
29. Cocker, R. P.; Chadwick, D. L.; Dare, D. J.; Challis, R. E. Int J Adhes Adhes 1998, 18, 319.
30. Lovell, R.; Windle, A. H. Polymer 1990, 31, 593.
31. Challis, R. E.; Freemantle, R. J.; Cocker, R. P.; Chadwick, D. L.; Dare, D. J.; Martin, C.; Mahendrasingham, A.; Fuller, W. Plast Rubber Compos 2000, 29, 109.
32. McSkimin, H. J. In Physical Acoustics; Mason, W. P., Ed.; Academic: New York, 1964; Vol. 1A.
33. McCrum, N. G.; Read, B. E.; Williams, G. Anelastic and Dielectric Effects in Polymeric Solids; Wiley: New York, 1967.
34. Cole, K. S.; Cole, R. H. J Chem Phys 1941, 9, 341.
35. Maistros, G. M.; Bucknall, C. B. Polym Eng Sci 1994, 34, 1517.